Velocity Field of a Lifting Rotor Blade in Hover

N. M. Komerath,* T. L. Thompson,† O. J. Kwon,‡ and R. B. Gray§
Georgia Institute of Technology, Atlanta, Georgia

Detailed measurements have been made using a laser velocimeter in the close vicinity of a lifting, single-bladed model rotor blade in simulated hover conditions to validate codes for predicting rotorcraft aerodynamics. Data acquired at a rotor tip speed of 32 m/s and a tip Reynolds number of 2.7×10^5 are compared with predictions made using a thick-bladed panel code coupled to a prescribed wake calculation. Rotor inflow measurements are seen to agree closely with panel code results, even when examined with high chordwise resolution. Agreement is less definite in the near wake, where strong tip vortex effects are felt, and the vortex core model becomes important. Tip vortex formation is clearly visible from the data. Deviations from periodicity are insignificant in the close vicinity of the blade. Particle spin-out effects are seen to be pronounced in the vortex core when using conventional seeding materials but to be greatly reduced by the use of incense seeding. The precise measurement of vortex core velocity profiles is seen to be within reach.

Introduction

THE wake of a helicopter rotor involves a system of vortices shed from the blade tips, vortex sheets shed from the blade trailing edges, and a vortex system shed from the blade roots, as shown in Fig. 1a.[1] The mutual interactions of these systems and their geometric and temporal complexities make this a challenging flowfield to predict and measure. Since the rotor operates in very close proximity to and even inside this flowfield during the crucial phases of landing and hovering, rotorcraft performance is quite sensitive to wake conditions. Best known among rotorcraft aerodynamic prediction tools are the vortex-based methods, where the wake is modeled as a system of vortices, inducing velocities on themselves and on the rest of the flowfield. The induced velocities are then used to find the loads on the rotor blades. The success of these methods stems from the fact that the rotor blade tips encounter the highest dynamic pressure and account for a significant fraction of the thrust generated as well as the losses suffered. The tip vortices are dominant features of the rotor wake. Accurate computation of the velocities induced by the tip vortices can yield accurate prediction of blade loads. Two vortex wake methods are in use: prescribed wake analysis[2] and free wake analysis.[3] In prescribed wake codes, the tip vortex geometry is specified, having been determined from empirical databases, generated from flow-visualization studies. Blade load results obtained by using this method agree well with experiments, but obviously there are severe disadvantages when new blade geometries are used. The free wake analysis also starts from some initial specification of an approximate vortex geometry and inflow but then iterates until a converged geometry is found. However, in general, the converged wake geometry and predicted velocity field turn out to be significantly different from reality. In addition, the inflow to the rotor plane is complex, and its modeling requires verification.

More recent efforts to model rotorcraft aerodynamices use the full-potential,[4] Euler,[5] and Navier-Stokes[6] approaches to compute the flow near the rotor blades in detail. Most code development efforts and experimental programs in this area have focused on rotor blade loads; hence, surface pressure distributions are far more common than velocity field measurements. These are inadequate to tackle problems such as blade-vortex interactions, tip shape effect modeling, rotor-airframe aerodynamic interactions, and rotor-wing interactions. This provides added motivation to undertake an extensive experimental investigation of a flowfield simple enough to validate analytical models in manageable steps.

The flowfield in the near wake of a spinning rotor involves steep velocity gradients, flow reversals, and rapid periodic and unsteady variations. Intrusive probes cannot be used very close to the rotor and can cause significant interference in vortices. Even with optical diagnostics, several problems are encountered. However, it has proved to be possible to compile a set of detailed measurements with good accuracy.

Several studies of rotary wing flowfields have been conducted using the laser Doppler velocimeter (LDV). Biggers and Orloff[7] measured the drag of a rotor in forward flight in a wind tunnel using the momentum deficit downstream of the rotor. Landgrebe and Johnson[8] performed extensive measurements of the flow around a helicopter to study the rotor wake. Desopper[9] measured the flow around a rotor in forward flight at transonic tip Mach numbers. Mba et al.[10] have investigated the effect of tip shapes on the radial load distribution. They computed circulation at radial stations from integrated velocity data. Owen and Tauber[11] studied the wake of a rotor spinning at high speeds in hover to validate acoustics prediction codes. In addition, there have been many related studies[12,13] on propeller flowfields.

The present study aims to develop a simple and detailed test case for the development and validation of prediction codes. Simplicity comes from the constant-chord, untwisted geometry of the single blade and the absence of compressibility effects. The vortex systems from multiple blades interact in complex ways. Iterative computation of these interactions is the expensive part of wake prediction, therefore, detailed examination of accuracy is inhibited by cost. High Mach number is doubtless of importance to aerodynamic, aeroelastic, and aeroacoustic predictions, but the incompressible vortex field in the near wake has not yet been predicted precisely by any code. There is also a previously obtained body of data[14] on the pressure distribution near the tip of this rotor. High chordwise resolution is sought here; and measurements are attempted close to the blade surface to make code validation easier. The techniques developed here are to enable detailed measurements of the vortex core. Laser velocimetry is, by no means, routine for such flowfields: several difficult problems remain, and each experiment has to be carefully set up to avoid large errors. The simple geometry permits close examination of the accuracy and prob-

Received April 5, 1987; revision received July 6, 1987.

*Assistant Professor, School of Aerospace Engineering. Member AIAA.

†Graduate Fellow, School of Aerospace Engineering; currently with McDonnell Douglas Helicopter Company, Mesa, AZ. Student Member AIAA.

‡Graduate Research Assistant, School of Aerospace Engineering. Student Member AIAA.

§Regents' Professor, School of Aerospace Engineering. Member AIAA.

lems in such measurements, and some of these issues are resolved in this work. Extension of such detailed measurements to higher tip speeds and compressible vortex fields is a future step, which will be taken in large facilities, but must take lower priority here than extension to low-speed forward flight cases.

Facility Description

The test facility is shown in Fig. 2. A horizontal rotor shaft is enclosed in a 2.7 × 2.7 m test cell. A wake inductor mounted in the center of a 10-mm mesh honeycomb screen provides for unrestricted flow of the rotor wake as well as smooth return of air into the inflow plane of the rotor, as verified by previous flow-visualization studies.[15] Test conditions were limited to those that produced an unobstructed flowfield by examination of velocity data in the current program. The single-bladed, untwisted rotor shown in Fig. 1b is of radius 0.6 m and constant chord of 0.127 m, with an NACA 0012 section and a square, flat tip. Pressure transducers at the tip and strain gages in the hub have been used in the past to compile a database on thrust, torque, and surface pressures on this blade.[14] A pitch link enables manual setting of blade pitch angle, and the blade is free to flap through 10 deg. In these tests, the coning angle was less than 0.1 deg.

A TSI 9100-7 two-component LDV system is used with a 5-W argon ion laser. An 8.5× beam expander facilitates measurements using lenses of focal lengths of 1500 and 2186 mm in backscatter. The front focusing lens can be traversed with 25-μ resolution inside a volume 600 × 600 × 750 mm using an optical traverse arrangement. The measurement volume is an ellipsoid 2 mm long and 0.1 mm in diameter in backscatter, and shorter when off-axis collection is used. Bragg cells and variable-frequency shifters are used on both components. Doppler signals from scattering particles, sensed by photomultipliers, are passed to counter processors. The time for 16 cycles of the signal, measured with 1-ns resolution, is used to compute the velocity. A shaft encoder enables computation of the blade position at the instant of measurement of every data value.

Data Analysis

Data were collected in blocks of 500 validated measurements each. Each block was converted to a table of velocity component vs rotor azimuth and then sorted into 60 slots, each spanning 6 deg. The data in the three slots spanning blade passage across the azimuth of the measuring volume were then further sorted into 36 bins, each thus representing an interval of 0.5 deg. This was repeated 200 times, for a total of 100,000 validated measurements at each location. The data in each slot were then averaged. This procedure allowed unlimited numbers of measurements to be collected for statistical accuracy, but it prevented studying each revolution of the rotor in isolation, since only 500 points were taken in each batch.

Seeding Techniques

The LDV measures the Doppler shift in light scattered by solid or liquid particles crossing the measurement volume. This means that 1) such particles must traverse this volume often enough to enable acceptable rates of data acquisition, 2) their injection must not change the flowfield significantly, 3) their size and optical properties must enable sensing of the scattered light with good signal-to-noise ratio, and 4) they must be small and light enough to move with velocities that are not different from the fluid velocity. These restrictive and contradictory requirements pose what is probably the most vexing practical problem confronting the experimenter who uses the LDV.

Artificial seeding was required. Strong jets could not be used to pump in seed material. Powders such as Al_2O_3 and TiO_2 were ruled out as health hazards unacceptable in the classroom building housing the facility. Polystyrene latex spheres cost too much. With these constraints, seeding techniques were studied. Initial efforts using atomized water and then a steam probe gave good signal quality but the size range was nonuniform, with too many large particles. Results with an ultrasonic nozzle were better, but the data rate was low and erratic (about 100 s^{-1}) due to rapid droplet evaporation.

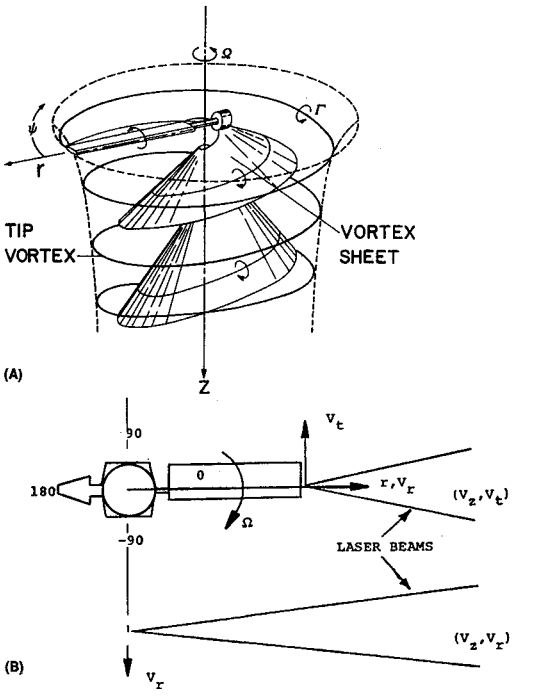

Fig. 1 a) Smoke study model of the hover flowfield,[1] b) rotor blade, measurement coordinates, and scheme for three-component measurement.

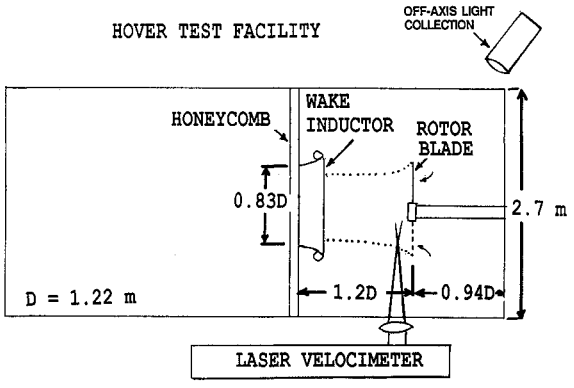

Fig. 2 Plan view of the facility.

Two successful solutions were developed. The first uses a simple atomizing nozzle, shown in Fig. 3, which generates a low-velocity cloud of mineral oil droplets. The fluctuation in signal amplitude is less than a factor of 4, indicating a narrow size range. They also remain suspended in quiescent air for long periods, indicating a low sink rate. Efforts to measure sink rate failed since random air motions exceeded the sink rate. This method of seeding has proved successful everywhere except in the viscous core of the tightly wound tip vortex, where the particles are seen to spin out. In addition, the closed-return facility allowed the seeder to be shut off during data acquisition. The second means of seeding involves the generation of incense smoke. These particles are much smaller and are hard to detect in the backscatter mode of light reception. However, they do follow the flow even in the viscous core of a vortex. With incense sticks distributed throughout the facility, a uniformly seeded flowfield could be produced without the need for seeding jets, but curious visitors had to be warded off.

Estimates of seed particle size were gaged by observations of signal amplitude in another facility. These indicate that the mineral oil droplets are about twice as large as the 1-μ aluminum oxide used there. By the same comparative technique,

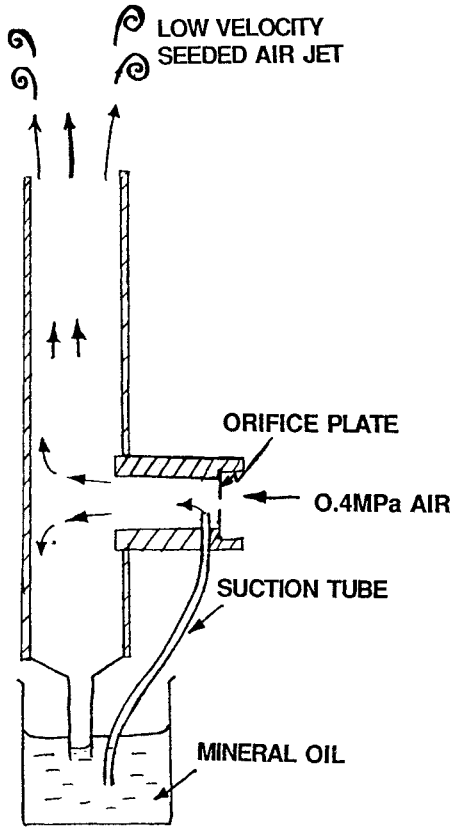

Fig. 3 Lauterbach-type atomizer seeder.

the incense smoke is on the order of 0.2 μ. More precise measures were not made. The velocity data are independent of particle size provided that acceleration effects are negligible. This applies to the mineral oil, except in the vortex core.

Spin-out effects may be partially gaged from the probability of sensing a particle in different parts of the flowfield. In Fig. 4, the particle arrival distribution is plotted as a function of rotor azimuth. The ordinate is normalized using the average number of particles per azimuth slot. Two effects are significant. First, more particles are sensed in slots where the fluid moves faster through the measuring volume. This effect is seen in the rise in the distribution as the rotor blade passes. Second, few particles are sensed in the vortex core, where they spin out due to centrifugal effects. This is clearly evident in the case of the mineral oil seeding, where few particles are sensed while the vortex core passes. Often, no data points could be acquired during the six degrees of core passage even when a total of 100,000 points were acquired. When incense seeding with off-axis light reception was employed, this effect was reduced to the point of being indistinguishable from the velocity bias effect. The occurrence of the spin-out also results in large differences in arrival rate between the two techniques, but very little difference in the velocity data shown for the same conditions, outside the core.

The particle defect occurred only at locations intersected by the tip vortex core when mineral oil seeding was used. Thus, this seeding was used to perform measurements everywhere except in the vortex core, where incense seeding and off-axis scatter had to be employed. This latter work will be reported later. The particle defect is also a reliable means of identifying passage of the vortex core.[16,17]

Unsteadiness in the Flow

It is assumed in the data analysis that the flowfield is periodic and synchronized with the rotor. However, unsteadiness has been reported by other researchers.[18] To test for the occurrence of such effects, the histogram of the data occurring within a 0.5-deg azimuth interval was used. No evidence of bimodality, which would indicate the presence of organized oscillations,

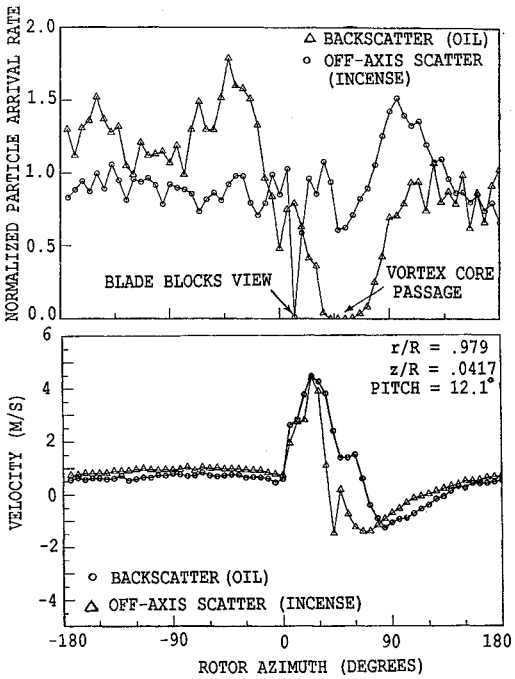

Fig. 4 Particle arrival distributions at a location intersected by the vortex core, and the corresponding axial velocity measurements, obtained using mineral oil and incense seeding.

was found. The histograms showed some scatter beyond the delta function, which might have been expected had the flow been perfectly steady and uniform, because of 1) the rate of change of velocity with varying azimuth, which produces variance in any discrete interval, 2) nonuniformity in particle size, and 3) turbulent fluctuations. The separation of effects 1–3 is beyond the scope of the present paper, since it requires simultaneous single-particle sizing and velocity measurement.

Experiments

Test Conditions

All tests reported here were run at 500 rpm, corresponding to a tip speed of 32 m/s. This was chosen to eliminate problems with the return flow in the facility. The low tip Reynolds number of 2.7×10^5 and low blade aspect ratio make the test conditions unrealistic as scale-model tests but make computation using Navier-Stokes simulation less expensive. Two thrust coefficients were used, 0.0057 and 0.0022, corresponding to collective pitch settings of 12 and 6.2 deg, respectively. The seeder was located far upstream of the rotor plane, and the cloud of mineral oil had peak velocities less than 10 cm/s in the flowfield. The absence of seeder interference was verified by comparison of data taken with the seeder on and off.

Close-to-Blade Measurements

The objective here was to obtain good chordwise resolution for comparison with analyses. The measurement volume was held at specified distances from the blade quarter-chord plane. The data arriving when the blade passed by the measuring volume were sorted into 0.5-deg intervals, so that approximately 24 chordwise points were obtained. The measurement points are all outside the blade boundary layer and are actually in planes parallel to the rotor tip path plane, not to the blade surface or chord. Gaps exist in this data, since the blade sometimes obstructed the laser beams. This causes no error in the data, since the Doppler frequencies corresponding to blade surface velocity were far removed from those corresponding to the flow velocity outside the boundary layer, and could be filtered out in the software: it was verified that no such data were collected. The blade surface was painted flat black to minimize surface scattering, and a field stop system was used in

the LDV to eliminate extraneous light; the combination proved effective.

Three-Component Measurements

The LDV measures only the two velocity components perpendicular to its optical axis. In the hover flowfield, assumption of axial symmetry is valid, and the vertical velocity component can be used as either the tangential component, when the blade is horizontal, or the radial component when the blade is vertical. In both cases, the horizontal component is directed along the axis of the rotor and serves as the means of validating the axial symmetry assumption. Initially, the LDV was operated as a two-component system. While data quality was good, signal amplitude was low, and the rate of data acquisition averaged only about 300/s, being limited by the signal-to-noise ratio in the 488 mm channel. To improve this situation, the LDV was reconfigured as a one-component system. Indicent line intensity was increased, and loses were reduced removing the color separator and filters. Signal quality improved, and steady data rates of 3000/s became easy to achieve. Subsequent runs were made one component at a time.

Preliminary Vortex Core Measurements

To demonstrate the feasibility of vortex core velocity measurements, off-axis scatter-receiving optics were used. Incense seeding was employed to minimize spin-out effects. Vortex passage locations were identified by minimal particle arrival probability when using mineral oil. Figure 5 shows the velocity traces obtained at one such location. Since the receiving optics system had to be realigned for each measurement location, few such measurements could be made. However, the data showed excellent repeatability between runs, showing that precise location of the vortex and measurement of the velocity profile in the core were within reach. These velocity components are relative to a stationary observer. Resolution into components aligned with the moving vortex requires knowledge of the precise vortex trajectory and a large number of vortex core measurements. These require an automated system to move the receiving optics and keep them aligned with the transmitting optics.

Data Validation

Initial alignment was performed before each set of runs using a stationary solid surface and a frequency shift of 1 MHz. The alignment was tuned until the data rate reached the counter limits, as determined by the time per measurement and the reset time. Next, the seeder shown in Fig. 3 was used to provide a repeatable air jet seeded with mineral oil. Signal quality was tuned to standardized conditions. Signal quality was monitored during actual operation, and the entire operation was repeated when quality was seen to deteriorate. Velocity histograms measured using solid surfaces and the seeder jet were examined to ensure rejection of spurious values, and amplifier gains were adjusted accordingly. Frequency shift was then used to measure the mean velocity in the test cell with the seeder shut down and the air quiescent. Typical errors were found to be less than 10 mm/s. The fringe spacing of the LDV was checked by actual measurement of the beam-crossing angle. Measuring volume size was checked using the traverse to determine the limits within which a solid surface could produce a signal. In a different facility (a wind tunnel), the same LDV system was checked against a pitot-static probe. The mean agreed to within 0.1%. Comparison with a hot wire yielded the expected result that the LDV could not measure turbulence intensities below about 0.5%, while the hot wire measured about 0.3%.

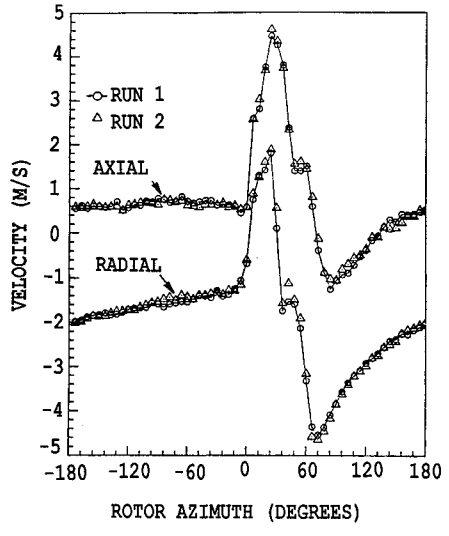

Fig. 5 Repeatability of measurements made at a location intersected by the tip vortex periodically. Secondary features are visible in the inner core.

Analytical Predictions

The measurements were compared with computations made with the thick-bladed hovering rotor analysis initially developed by Shenoy and Gray,[19] which had already shown excellent agreement with measured blade surface pressure distributions for this rotor.[14] The code was extended to predict the induced velocity field above and below the rotor disk plane. The blade upper and lower surfaces with a half-body of revolution tip (the experimental blade had a flat tip with sharp edges) were represented by curved panels. A vortex sheet with linearly varying spanwise (α) and chordwise (β) components of vorticity was assumed across each panel. The blade bound circulation distribution was obtained by integrating the spanwise velocities along the chord at each spanwise station. A "freestream vorticity" directed along the axis of rotation was added to the blade surface vorticity to shift coordinates to the blade. The wake was represented by a single tip vortex equal in strength and outboard of the maximum bound circulation and by trailing vortex filaments inboard.

Determination of Wake Geometry

A prescribed wake/lifting-line method was used to determine the tip vortex geometry. The inboard trailing vortex filaments were located iteratively. The tip vortex geometric parameters were obtained from Ref. 20 for the specified thrust coefficient. The approximate initial strength of the tip vortex determined from the measured ultimate wake geometry[21] enabled Biot-Savart computation of induced velocity at the blade lifting line. Using a lifting-line/blade element approach and the given collective pitch angle, the value of blade bound circulation distribution was determined, the tip vortex strength found, and the process was repeated to convergence.

Vortex sheet geometry was computed next. The intersection of the sheet with any azimuthal plane was assumed to be a straight line.[21] The outer edge of this inner sheet was assumed to leave the lifting line midway between the radial stations of 90% and maximum bound circulation. The ratio between the local radii of the outer edge and the tip vortex was held constant and the outer edge was allowed to move axially at the velocity induced by the tip vortex and the lifting line. The contracting surface thus generated was replaced by a finite number of vortex filaments. The induced velocity at the lifting line and the tip vortex strength were recomputed, and the procedure was repeated until a converged solution was obtained for the trailing vortex geometry and the lifting-line circulation distribution. For the lifting-surface calculation, the trailing vortex filaments were forced to leave the blade trailing edge at the same radial stations as from the lifting line. The geometry was fixed except for the near-wake tip vortex, which was allowed to move to permit empirical modeling of tip vortex formation and roll-up.

Computational Details

The induced-velocity integration in the lifting-line calculation was performed in radial planes spaced at 10-deg azimuthal intervals in 10-deg steps of blade rotation for four blade revolutions. The points so determined were connected with straight-line vortex elements. Five trailing vortex filaments were used for the lifting-line calculations and eight for the thick lifting-surface case. The blade surface was broken into 13 spanwise and 19 chordwise panels on both the upper and lower surfaces. A total of 570 panels were used, with a higher panel density near the tip. The problem was solved iteratively through the vorticity redistribution procedure, using the Biot-Savart law to compute the total tangential velocity vector at each control point on the blade surface panels. The initial spanwise vorticity distribution over the panels was obtained from the two-dimensional (2-D) potential method using the effective angle-of-attack distribution from the lifting-line calculation. The initial distribution of chordwise vorticity was obtained using continuity of vorticity. The collective pitch angle was adjusted to give an effective pitch angle in order to account for the difference between the actual and ideal values of 2-D lift-curve slope.

The near-field tip vortex left the tip at the quarter-chord point and was forced to join the far-field section of the tip vortex 15 deg after the blade pitch axis. This vortex section was free to move with the induced velocity due to the whole vortex system during the iteration process to find a "force-free" condition. Its strength was assumed to grow linearly from zero at the tip separation point to full strength at the matching point. Since the wake geometry was specified and an initial vorticity strength distribution was known, the total tangential velocity vector at each panel control point on the blade surface could be evaluated and used to determine a new set of vorticity strengths. This iterative process was continued until an acceptable convergence was obtained[22]. The velocity field induced by the converged vortex system was used to calculate the variations at fixed measuring locations.

Results and Discussion

Bias Effects

Laser velocimetry is subject to various bias effects that must be accounted for. The velocity bias effect occurs when digital acquisition of a fixed number of points is performed, because more of these points will be acquired during periods when the velocity is high and more particles traverse the measuring volume. However, in these measurements, this error does not occur because ensemble averaging is performed inside each azimuth interval, so that the numbers in each interval do not affect any other interval. A fringe bias occurs when small particles fail to cross a sufficient number of bright fringes to trigger a measurement. This is minimized by the use of frequency shift, which has the effect of moving the fringes at high speed relative to the particles. A similar effect can occur if there are large variations in velocity, as in a vortical flow. Again, this is avoided by the use of frequency shift.

Repeatability

Figure 5 demonstrates the repeatability of the measuring locations, system alignment, and run conditions under the most stringent conditions, where the tip vortex core is intersected. Even the secondary features evident in the core are repeated. At this time, the reasons for these secondary features are not well understood, but they are definitely features of the flow and not the measurement or analysis.

General Flow Features

All of the results presented are in the stationary reference frame, as shown in Fig. 1b. This choice of reference frame is made for two reasons: first, this minimizes processing of the experimental data and presents it in a form closest to the raw data and, second, conversion to blade-fixed coordinates adds large constants to the data, making measured variations quite difficult to see. To validate codes, the analyst can easily transform results to the laboratory coordinate system and perform precise comparisons. The velocities are normalized using the momentum-theory value of induced velocity V_0, which is 1.71 m/s for the 12-deg pitch case and 1.07 m/s for the 6.2-deg pitch case, respectively.

A large database has been compiled, excerpts of which are shown here. Figure 6 shows the variation in the three components of velocity at a fixed position as the rotor goes through 360 deg of azimuth. The measurement plane is at $z/R = -0.0412$, where z is measured (see Fig. 1) normal to the plane passing through the blade quarter-chord line when the rotor is at rest (coning angle = 0). This plane is upstream of the rotor disk. The point is located inboard of the tip ($r/R = 0.876$). As expected, a strong, inward radial component is seen. The only significant tangential velocity occurs when the blade passes under the measuring point and creates a low-pressure or suction region. All components are greater in the quadrant of the disk following the blade passage and become larger as the measuring plane approaches the rotor plane.

The flow in the near wake is dominated by the tip vortex. The influence of the tip vortex is clearly evident in the radial/tangential vector plots shown in Fig. 7. The vortex induces a strong outward radial component at the edge of the disk until it passes through the measuring plane and begins to induce an inward radial component. As the blade passes, a strong tangential velocity, directed from the trailing edge to the leading edge of the blade, is seen. This is again physically due to the low pressure at the front of the blade and the high pressure behind, and is modeled as the "bound circulation." The axial velocity is also strongly influenced by the tip vortex. The edge of the disk experiences a strong upwash following the passage of the blade as the tip vortex is swept inboard of the measuring location. The largest upwash component was observed to occur when the radial component changed direction, which is reasonable since the largest axial velocity would be expected in close proximity to the tip vortex core.

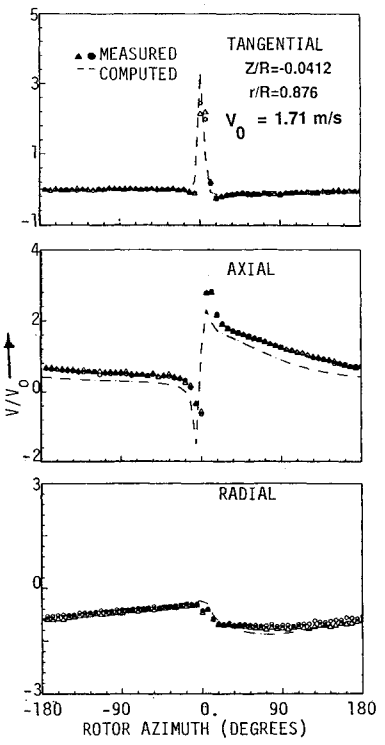

Fig. 6 Comparison of measured and predicted inflow velocities. Zero deg corresponds to the blade quarter-chord line crossing the projection of the measuring location on the tip path plane.

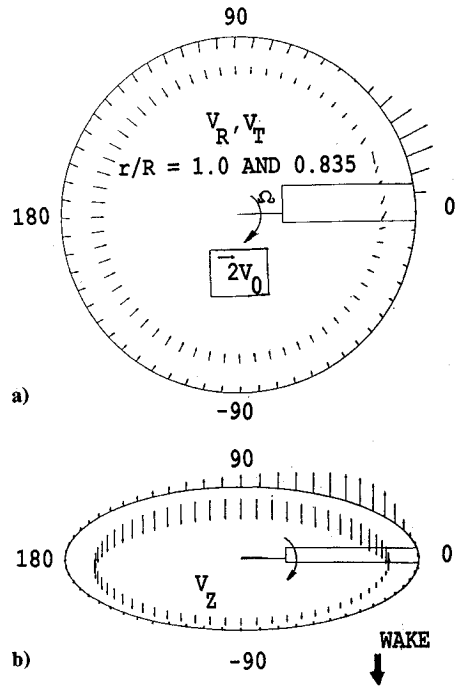

Fig. 7 a) Resultant of the tangential and radial velocity components at two radial locations, showing effects of blade passage and tip vortex intersection, b) axial velocity component. $V_0 = 1.71$ m/s in both cases.

Flowfield Near Blade

Three components of velocity are plotted in Fig. 8a in a plane located at $z/R = -0.309$. The velocity is shown as a function of the blade azimuth with the angles corresponding to the passage of the leading edge and trailing edge of the blade indicated on the figure. High chordwise resolution is obtained using 0.5-deg azimuth resolution, which gives more than 20 stations between the trailing and leading edges. Chordwise resolution is limited by the number of data values required in each bin to obtain a stable average. With a total of 100,000 points acquired, each 0.5-deg bin collects over a hundred data values before averaging. This is seen to be adequate to obtain consistent data.

Qualitative views of the flow close to the blade can be gained from Fig. 9, where vectors representing the radial and tangential components measured in five axial planes are shown. Three of these planes are upstream and two are downstream of the rotor tip path plane. The closest upstream plane shows the flow moving inboard as the tip vortex forms at the quarter-chord line. The planes further upstream show better defined radial inflow. On the downstream side, the closest plane shows a clear region of demarcation between the radial outflow forming the tip vortex and the radial inflow further inboard, which will form the trailing vortex sheet. The tangential velocity exhibits the expected behavior of the "bound circulation."

Figure 10 shows the resultant of the axial and radial components, represented as vectors in planes perpendicular to the tip path plane. The objective here is to visualize the tip vortex. The plane intersecting the quarter-chord line shows the vortex just beginning to form. The other planes, intersecting the blade at downstream stations, show a considerably strengthened vortex, with the downward component of the vectors increasing above the upper surface of the blade. The gaps in the plots are regions where data could not be obtained because of the blade blocking one or both incident laser beams. It is to be noted that each vector shown here actually represents the velocity at a different age of the vortex, and, hence, streamlines cannot be connected through them. The vectors represent the periodic part of instantaneous velocity in planes cutting the moving

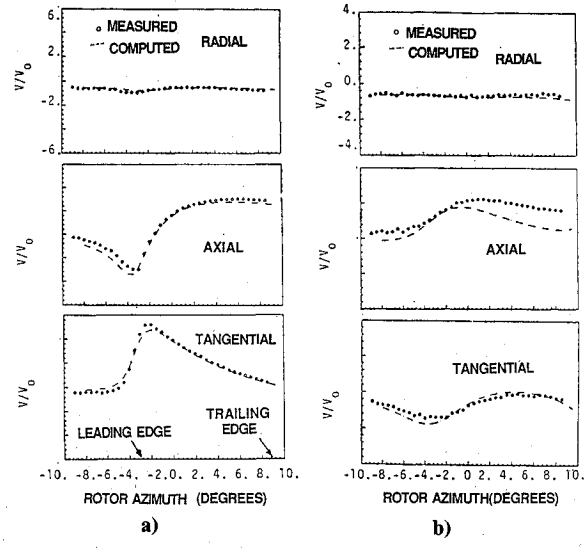

Fig. 8 Comparison of measured and computed velocity components during blade passage at inflow a) ($z/R = -0.0412$) and b) wake ($z/R = 0.0412$) locations. $V_0 = 1.71$ m/s, $r/R = 0.876$.

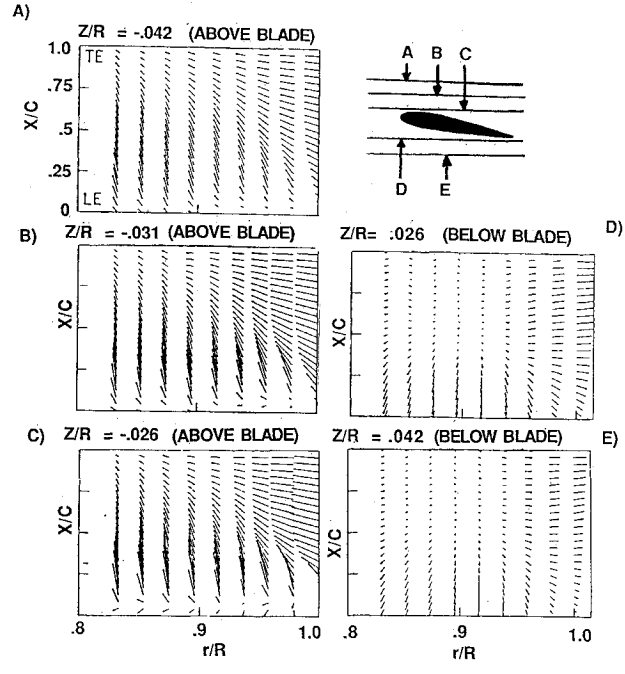

Fig. 9 Projected velocity in planes parallel to the tip path, upstream (a, b, c) and downstream (d, e). Note demarcation between inward and outward spanwise velocity in d) and tip vortex formation.

vortex. The generation of trajectories in the vortex requires interpolation of data from different planes and subsequent three-dimensional processing. These will be reported in a subsequent paper.

Circulation

To determine the circulation at different spanwise locations on the blade, the measured velocity was piecewise integrated over contours enclosing the blade. Three contours, at different distances from the upper surface of the blade, were chosen in order to examine the sensitivity of this computation to the choice of contour. Figure 11 shows that, at the tip region, the measurement is sensitive to the choice of location, so that significant amounts of vorticity cross the contours. However, inboard, this method provides a good measure of bound

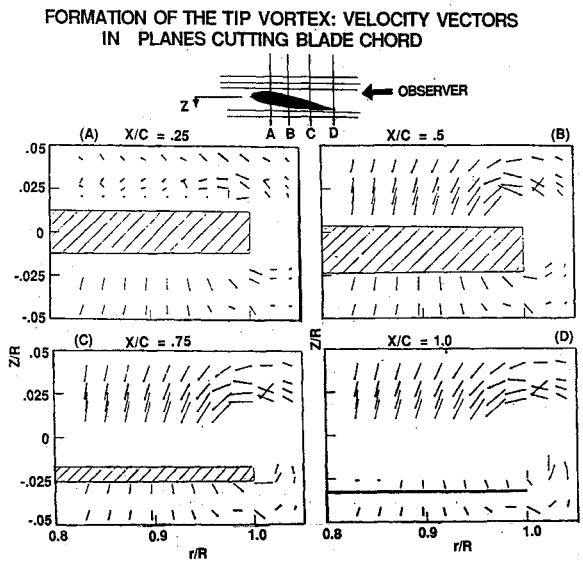

Fig. 10 Projected velocity in planes perpendicular to the tip path over the outboard 20% of the blade. Blade intersections are hatched. Velocity vectors inside the core are not shown.

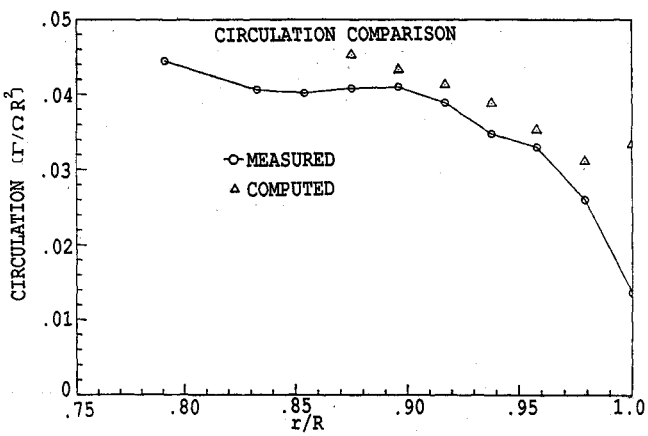

Fig. 11 Measured and predicted values of bound circulation. Sensitivity to choice of contours causes measurement error outboard of $r/R = 0.9$.

vorticity. Agreement with the analysis is also good at these inboard locations.

Limitations of the Experimental Technique

While the data exhibit excellent repeatability and consistency, certain limitations must be noted by those performing code validation. The error in measured mean quantities is very small (each velocity component accurate to within 10 mm/s), but measurements made off single particles have not shown reliable accuracy and, hence, statistical averaging has been essential. Velocity traces from successive blade revolutions cannot be accurately obtained and compared at present. Turbulent and other random fluctuations have been averaged out, although slot variance data has been stored for every slot. Flow visualization[17] has since demonstrated the repeatability between revolutions to be good, but this cannot be claimed from the LDV data alone. The error due to particle lag and nonuniform particle sizes has not been verified quantitatively. They are believed to be negligible everywhere outside the vortex core, based on observations of sink rate in quiescent air, but again precise measurements of this error are lacking. Measurements have not been attempted inside the boundary layer of the blade. The large focal length of the system, and the associated length of the measuring volume, mean that the present optical arrangement is not optimized for such measurements.

Code Validation Results

The velocity field predicted by the thick-bladed panel code was compared to the measurements. Certain differences exist between the analytical and experimental models. First, the tip was modeled as a half-body of revolution for ease, and a core model was used. Second, the walls and honeycomb of the facility were not modeled, and the rotor was assumed to be in an unconfined space. Third, the details of the hub and the counterweight were not modeled. Figure 6 shows comparison between the computed and measured velocity field in the inflow region over one revolution of the blade. The tangential and radial components of inflow are modeled accurately, but there is a consistent difference in the axial component. Figure 8a shows comparisons of the inflow velocity during blade passage. Agreement is excellent, but is poorer in the wake, shown in Fig. 8b, because of the core model used. These general results held true at other stations as well, with the inflow velocities being predicted with high precision, and the wake velocities showing disagreement, especially at the tip region shown in Fig. 8b.

Conclusions

1) Laser velocimetry has been used to obtain detailed measurements of the periodic velocity field in the close vicinity of a single-blade rotor in hover. These measurements have been used to construct qualitative views of the velocity field, as well as quantitative comparisons with an existing prediction code, which has been modified to compute the velocity field.

2) Seeding of this flowfield is a crucial consideration due to the presence of high values of spatial and temporal rates of change, and the use of large focal lengths. For this application, seeding using atomized mineral oil has proved to be highly successful, except in the tip vortex core, where incense seeding and off-axis scatter reception were found to be essential.

3) Evidence of unsteadiness has been sought, and none has been found, in the near wake. The measurements show excellent repeatability and low data scatter.

4) Measurements close to a moving blade have been demonstrated, as have measurements inside the core of the moving tip vortex. Secondary features have been observed inside the vortex core, for which a complete explanation is not available at present. The data close to the blade show the effects of the bound circulation, the formation of the tip vortex, and the subsequent growth and separation of the vortex.

5) The thick-bladed panel code developed by Wey and Gray has been extended to perform computations of induced velocity at space-fixed locations close to the rotor. An empirical model of the tip vortex core has been used, along with an initial prescribed wake geometry. The predictions show excellent agreement with the experimental data in the inflow region and at inboard stations in the near wake; however, agreement is less precise at the tip region, where the tip vortex effects are pronounced. The importance of accurately modeling the tip vortex is clearly demonstrated. The close agreement between the panel code results and the inflow velocity data also indicates that the present measurements are not significantly affected by the presence of the facility walls and, hence, is suitable for inexpensive code validation without the need for modeling the walls.

6) A data set has thus been developed and used for validation of codes to predict the flowfield close to a spinning rotor blade in hover.

Acknowledgments

The authors gratefully acknowledge the support of this work by the U.S. Army Research Office as part of the Center for Rotary Wing Aircraft Technology, Contract DAAG29-82-K-0094, monitored by Dr. Robert E. Singleton.

References

[1]Gray, R. B., "An Aerodynamic Analysis of a Single-Bladed Rotor in Hovering and Low-Speed Forward Flight as Determined from Smoke Studies of the Vorticity Distribution in the Wake," Princeton

University Aeronautical Engineering Department, Rept. 356, Sept. 1956, p. 65.

[2]Kocurek, J. D. and Tangler, J. L., "A Prescribed Wake Lifting Surface Hover Performance Analysis," *Journal of the American Helicopter Society*, Vol. 22, Jan. 1977, pp. 24–35.

[3]Landgrebe, A. J., "An Analytical Method of Predicting Rotor Wake Geometry," *Journal of the American Helicopter Society*, Vol. 14, Oct. 1969, pp. 20–32.

[4]Egolf, T. A. and Sparks, S. P., "A Full-Potential Rotor Analysis with Wake Influence Using an Inner-Outer Domain Technique," *Proceedings of the American Helicopter Society 42nd Annual Forum*, June 1986, pp. 997–1012.

[5]Sankar, L. N. and Tung, C., "Euler Calculations for Rotor Configurations in Unsteady Forward Flight," *Proceedings of the American Helicopter Society 42nd Annual Forum*, Washington, DC, June 1986, pp. 985–996.

[6]Wake B. E. and Sankar, L. N., "Solutions of the Navier-Stokes Equations for the Flow About a Rotor Blade," presented at the AHS Specialists' Meeting on Aerodynamics and Aeroacoustics, Arlington, TX, Feb. 1987.

[7]Biggers, J. C. and Orloff, K. L., "Laser Velocimeter Measurements of the Helicopter Rotor-Induced Flow Field," *Proceedings of the 30th Annual Forum of the American Helicopter Society*, May 1974.

[8]Landgrebe, A. J. and Johnson, B. V., "Measurement of Model Helicopter Rotor Flow Velocities with a Laser Velocimeter," *Journal of the American Helicopter Society*, Vol. 19, No. 3, July 1974, pp. 39–43.

[9]Desopper, A., "Rotor Wake Measurements for a Rotor in Forward Flight," *Proceedings of the First International Conference on Rotorcraft Basic Research*, Research Triangle Park, NC, Feb. 1985.

[10]Mba, M. N., Meylan, C., Maresca, C., and Favier, D., "Radical Distribution Circulation of a Rotor in Hover Measured by Laser Velocimeter," Paper 12, Tenth European Rotorcraft Forum, Aug. 1984.

[11]Owen, F. K. and Tauber, M. E., "Measurement and Prediction of Model-Rotor Flow Fields," AIAA Paper 85-1558, July 1985.

[12]Lepicovsky, J. and Bell, W. A., "Aerodynamic Measurements About a Rotating Propeller with a Laser Velocimeter," *Journal of Aircraft*, Vol. 21, April 1984, pp. 264–271.

[13]Kobayashi, S., "Propeller Wake Survey by Laser-Doppler Velocimeter," *Laser Anemometry in Fluid Mechanics*," Selected Papers from the First International Symposium on Laser-Doppler Anemometry to Fluid Mechanics, LADOAN–Instituto Superior Tecnico, Lisbon, Portugal, July 1982, pp. 195–208.

[14]Gray, R. B., McMahon, H. M., Shenoy, K. R., and Hammer, M. L., "Surface Pressure Measurements at Two Tips of a Model Helicopter Rotor in Hover," NASA CR-3281, 1980.

[15]Shivananda, T. P., "Pressure Measurements Near the Tip of a Hovering Model Rotor Blade and a Preliminary Investigation of the Flow in a Rotor Wake," Ph.D. Thesis, Georgia Inst. of Technology, School of Aerospace Engineering, Dec. 1977.

[16]Thompson, T. L., "Velocity Measurements Near the Blade Tip and in the Vortex Core of a Hovering Model Rotor," Ph.D. Thesis, Georgia Institute of Technology, School of Aerospace Engineering, Dec. 1986.

[17]Thompson, T. L., Kwon, O. J., Kemnitz, J. L., Komerath, N. M., and Gray, R. B., "Tip Vortex Core Measurements on a Hovering Model Rotor," AIAA Paper 87-0209, Jan. 1987.

[18]Carradonna, F. X. and Tung, C., "Experimental and Analytical Studies of a Model Helicopter Rotor in Hover," USAAVRADCOM TR. 81-A-23, Sept. 1981.

[19]Shenoy, K. R. and Gray, R. B., "Iterative Lifting Surface Method for Thick-Bladed Hovering Helicopter Rotors," *Journal of Aircraft*, Vol. 18, June 1981, pp. 417–424.

[20]Wey, T. C., "A Numerical Analysis for Blade Tip Loadings on a Thick Bladed Hovering Helicopter Rotor," Ph.D. Thesis, Georgia Inst. of Technology, School of Aerospace Engineering, Dec. 1983.

[21]Gray, R. B. "On the Motion of the Helical Vortex Shed from a Single-Bladed Hovering Model Helicopter Rotor and Its Application to the Calculation of the Spanwise Aerodynamic Loading," Princeton Univ., Aero. Engineering Dept. Rept. 313, 1955.

[22]Samant, S. S. and Gray, R. B., "A Semi-Empirical Correction for the Vortex Core Effect on Hovering Rotor Wake Geometries," *Proceedings of the 23rd Annual National Forum of the American Helicopter Society*, May 1977, pp. 02-1–02-10.